Simulation and Predictability in a Coupled TOGA Model

PETER R. GENT AND JOSEPH J. TRIBBIA

National Center for Atmospheric Research, Boulder, Colorado

(Manuscript received 29 April 1992, in final form 29 March 1993)

ABSTRACT

A model of the tropical ocean and global atmosphere is described. It consists of an aqua-planet form of version one of the NCAR Community Climate Model coupled to a primitive equation model for the upper tropical ocean in a rectangular basin. A 24-year simulation is described that has almost no climate drift, a good simulation of the mean temperature gradient across the ocean, but smaller than observed annual and interannual variability. The coupled model is analyzed to see where it occurs on the schematic bifurcation diagram of Neelin. In years 9–16 of the simulation there is a dominant oscillation with a period of two years. The spatial pattern of this oscillation shows up clearly in the first empirical orthogonal function calculated from monthly averages of sea surface temperature anomalies. A series of 19 model-twin predictability experiments were carried out with the initial perturbation being a very small change in the ocean temperature field. The correlation coefficient of monthly sea surface temperature anomalies from these model-twin experiments decreases rapidly over the first 6 months and after that, more slowly, showing that there is some predictability out to a year. The predictability times are marginally increased if only the coefficient of the first empirical orthogonal function of monthly averaged sea surface temperature anomalies or NINO3 sea surface temperature is predicted. There is some evidence to indicate that it is easier to predict the onset of a model warm event than to predict the onset of a model cold event. More detailed analysis of the first model-twin experiment shows that the initial divergence in the integrations is a change at day 6 in the incoming solar radiation due to a change in the atmospheric model clouds. The dominant early change in sea surface temperature occurs by this change in radiative heat flux. If the cloud feedback is set to zero, then the first changes are delayed to day 12 and occur in the evaporative and sensible heat fluxes and in the atmospheric wind stress. In this case the dominant early change to sea surface temperature is by advection due to the changed wind stress.

1. Introduction

One of the goals of the Tropical Oceans and Global Atmosphere (TOGA) program is to develop coupled atmosphere–ocean general circulation models (GCMs) that can be used to predict El Niño–Southern Oscillation (ENSO) events. At present, clear predictive skill has been demonstrated in a simple deterministic model (see Cane et al. 1986). Many scientific groups are working on coupled GCMs of the global atmosphere and regional models of the tropical Pacific Ocean. Most of these groups have their own atmospheric GCM, but many use the same ocean model: namely the Pacanowski and Philander (1981) modification of the Bryan and Cox Geophysical Fluid Dynamics Laboratory (GFDL) model. This work uses a version of the National Center for Atmospheric Research (NCAR) atmospheric GCM, called CCM1, and a new ocean model that was specifically designed for ENSO work.

This project was started when CCM1 was no longer being developed and the tropical ocean model was working only in a rectangular basin. So a coupled model was designed within these limitations that could be used to ask interesting questions about ENSO. The coupled model is an aqua-planet version of CCM1 coupled to the tropical ocean model in a rectangular basin. The main question to be addressed is, Do ENSO-like coupled oscillations occur in this model? The aqua-planet model does not have land–sea contrasts and is zonally symmetric so that it does not have an Asian monsoon or strong standing waves. In addition, the ocean model does not have the correct geometry of the tropical Pacific. Do these limitations mean that ENSO-like oscillations cannot occur?

Model-twin predictability experiments in atmospheric GCMs have become a standard technique to determine the limit of the model's predictability and to estimate atmospheric predictability. They have not been performed nearly so much with ocean GCMs. One reason is that the tropical ocean circulation is dominated by the forcing whereas the atmosphere is dominated by internal instabilities. In this situation predictability limits are governed more by the quality of the forcing and model-twin experiments make less sense. Several model-twin experiments with the new coupled GCM have been carried out; probably the first with a coupled GCM. These results are compared with those of Goswami and Shukla (1991), who performed model-twin experiments with the model of Zebiak and

Corresponding author address: Dr. Joseph J. Tribbia, NCAR, P.O. Box 3000, Boulder, CO 80307-3000.

Cane (1987). Blumenthal (1991) and Graham et al. (1992) have also addressed predictability in this model using a principal oscillation pattern analysis and using comparisons with observations in addition to model-twin experiments, respectively.

The layout of the paper is as follows. The coupled model is described in section 2. Section 3 describes a simulation run of the coupled model, and the results of the model-twin experiments are described in section 4. Section 5 contains more complete analysis of the first model-twin experiment, and the discussion and conclusions are in section 6.

2. The coupled ocean–atmosphere model

The NCAR Community Climate Model version 1 (CCM1) is thoroughly documented in Williamson et al. (1987). Several changes were made to this model before it was used in coupled mode, specifically, conversion to an aqua-planet configuration, a greatly simplified radiation calculation, evolving SSTs over the tropical Pacific, and a different wavenumber truncation.

CCM1 was converted to a perpetual January, aqua-planet version by removing the orography and treating the underlying surface as an ocean with zonally uniform temperatures. The sea surface temperatures (SSTs) for this aqua-planet run were determined by zonally averaging the standard CCM1 January surface temperature values. The surface roughness, z_0, used in this run is the standard CCM1 value over land of 0.25 cm. Zonal-mean averages of the solar and longwave radiation values at all 12 model levels were found as averages over the last 30 days of a 120-day run of the zonally symmetric aqua-planet integration.

For the coupled simulations, the radiation calculation was greatly simplified in the following manner. The values of solar and longwave radiation used in the atmospheric component of the coupled model are

$$\bar{Q}(y, z, t) = QS(y, z) + QA(y, z)\cos(2\pi t/365), \quad (1)$$

where t is time measured in days from 1 January and QS and QA are the symmetric and antisymmetric components about the equator tabulated from the last 30 days of the perpetual January aqua-planet run. In addition, in the coupled model the solar radiation at the surface over the interactive region of the rectangular ocean between 20°S and 20°N and 130°E and 80°W is modified as

$$Q(x, y, z = 0, t) = \bar{Q}(y, z = 0, t) \times [1 - 0.2F(x, y, t)], \quad (2)$$

where $\bar{Q}$ is given by Eq. (1) and F is the total cloud fraction determined by CCM1 using the cloud parameterization documented in Williamson et al. (1987). The coefficient of 0.2 in (2) is justified at the end of this section. It is necessary to have interactive clouds in the coupled model because cloud feedback on solar radiation is important for air–sea interaction in the tropics.

In the coupled runs, the SSTs over the interactive ocean are taken directly from the ocean model, and the surface roughness is given in meters by

$$10^4 z_0 = 1 + 0.2V, \quad (3)$$

where V is the surface wind speed in m s^{-1}. The SSTs and z_0 described above are smoothly interpolated to the standard aqua-planet values in the regions 100°E to 130°E, 80°W to 50°W, 20° to 30°N and S. Outside the region 30°S to 30°N, 100°E to 50°W the aqua-planet SSTs vary in a seasonal cycle determined by the monthly variation of the zonally averaged standard CCM1 surface temperature field.

CCM1 is often run with triangular truncation of 42 wavenumbers in the horizontal. Equatorial phenomena, especially in the ocean, have much longer zonal than meridional scales. Thus, the truncation was made trapezoidal to exclude some of the higher zonal wavenumbers while retaining 42 meridional wavenumbers. This enables a somewhat larger time step to be taken in CCM1. This modification and the greatly simplified radiation calculation means that the aqua-planet version of CCM1 used in the coupled calculations runs approximately twice as quickly as the full CCM1.

The upper equatorial ocean, primitive equation model is documented in Gent and Cane (1989). It is a reduced-gravity model using seven layers with a sigma coordinate in the vertical. It covers the volume between 130°E to 80°W, 30°S and 30°N down to an average depth of 400 m, which is the important region of the Pacific for ENSO on time scales no longer than a few years to a decade. The ocean below the isopycnal that forms the base of the active region is assumed to be at rest and of constant density. In the vertical the sigma coordinate is used to change between a depth coordinate for the upper, mixed layer and the bottom isopycnal.

The model has vertical mixing coefficients for momentum, ν, and heat, κ, which depend upon the local Richardson number. They are given in cm^2 s^{-1} by

$$\nu = 10^3/(1 + 10\,\mathrm{Ri})^2 + \nu_B$$
$$\kappa = 10^3/(1 + 10\,\mathrm{Ri})^3 + \kappa_B, \quad (4)$$

where the background values are 1–2 cm^2 s^{-1} for ν_B and 0.1–0.2 cm^2 s^{-1} for κ_B. This mixing is described in Gent (1991), which describes an application of the model in a rectangular basin with emphasis on the TOGA-COARE area of the western Pacific. The paper shows that the annual average heat flux into the ocean in the area 10°S to 10°N and 140°E to 180° is on the order of 10–15 W m^{-2}, which is much smaller than most estimates from observations.

The ocean model uses order 16 Shapiro filters for

horizontal dissipation. In the coupled model, two additional Newtonian frictions were included. The first was applied in the upper, mixed layer only. Surface horizontal velocities and (SST − 26°C) are damped with a Newtonian friction coefficient corresponding to a 180-day spindown time. We used 26°C because it is the zonal average of SST along the equator. A Newtonian form was chosen because it leaves the propagation characteristics of equatorial waves unchanged while reducing their amplitude with the 180-day spindown time. This friction was found necessary with the model forced by high-frequency atmospheric variability rather than monthly averaged fields, as was the case in the previous ocean-alone calculations. This mixed-layer Newtonian damping is clearly undesirable because it significantly damps SST anomalies over a year, which is only a fraction of the ENSO time scale, and this will inhibit coupled-model interaction. This frictional term is also not negligible in the ocean SST budget.

A further Newtonian damping on horizontal velocity was included near the western boundary of the model domain. The damping is applied at all levels with the coefficient decreasing linearly from that equivalent to a 7-day spindown time at the western boundary (130°E) to zero at 144°E. This western boundary friction is required in the coupled model because otherwise there is large, high-frequency variability in velocity at the western boundary, especially at about 7°–8°N and S. This is partially caused by the unphysical boundary waves of the bounded ocean model propagating toward, and concentrating variability at, the western boundary.

The atmosphere and ocean models are coupled synchronously as follows. CCM1 is run for a day with a time step of 20 minutes. Updated 7-day averages of wind stress and heat flux over the ocean domain, 130°E to 80°W and 30°S to 30°N, are calculated. This 7-day averaging of the atmospheric forcings can be thought of as a very simple model for the ocean mixed layer dynamics, which filters the high-frequency atmospheric forcing before transmitting it to the ocean below. These forcings drive the ocean model for a day with a time step of 45 minutes. The average ocean SST over that day from 20°S to 20°N and 130°E to 80°W is then smoothly interpolated to the climatology over the rest of the globe and passed back to CCM1. The cycle is then repeated. Note that the SSTs from only 20°S to 20°N are used because the SSTs poleward of these latitudes are too warm. The main reason for this is that the ocean model does not have the midlatitude gyres that act to reduce SSTs poleward of 20°S and 20°N. A brief description of an earlier version of the coupled model is given in Neelin et al. (1992), which contains a figure from a calculation made with the earlier version of the model.

The first runs of the coupled model were to test the interpolation scheme (described in section 2) around the edges of the ocean model domain. Then, a few more integrations were performed, varying the coefficients in formulas (2) and (3) that determine the effect of clouds on the heat flux and the surface roughness over the interactive ocean. The final values of the coefficients were chosen subjectively based on SST spatial patterns and lack of climate drift in the coupled-model calculations lasting several years. One of these integrations was for 11 years and the results are described in the model intercomparison of Neelin et al. (1992).

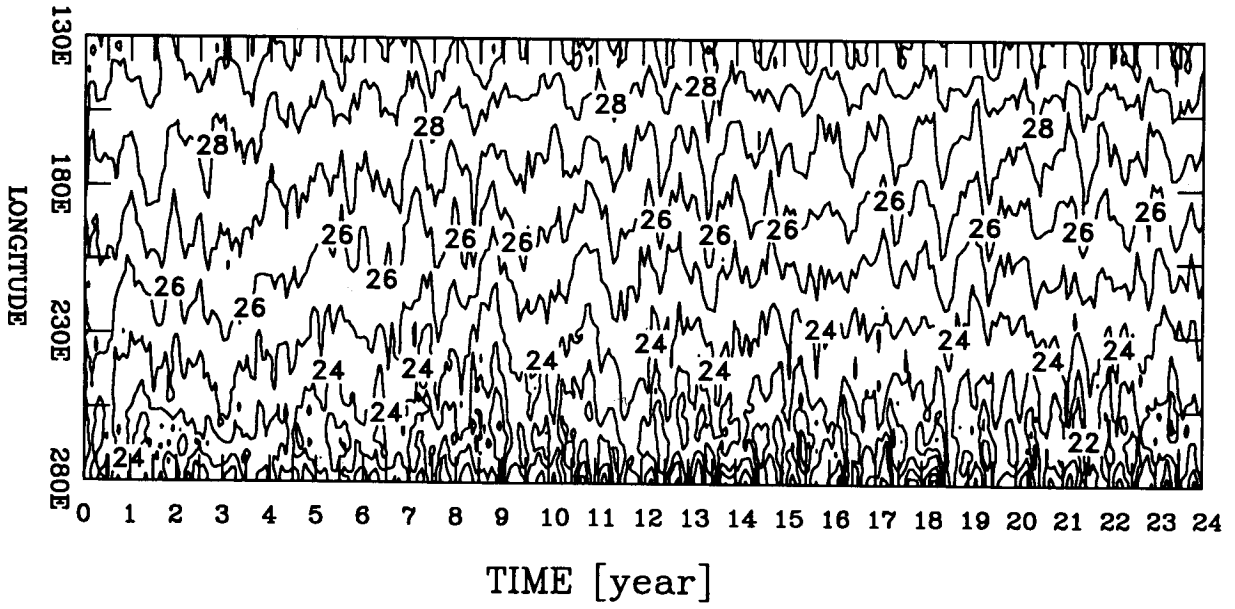

FIG. 1. The SST averaged between 1°S and 1°N along the equator versus time for the control run.

3. Simulation of the tropics in the coupled model

The final version of the coupled model was run for 24 years. The SST along the equator averaged between 1°S and 1°N is plotted against time for the whole run in Fig. 1. Several things are immediately apparent from Fig. 1: 1) there is very little climate drift in the model SST in 24 years, 2) the long-term average temperature gradient across the Pacific is captured quite well, and 3) no large El Niño events occur.

Figure 1 shows that the ocean SST along the equator cools over the first four years of the integration. In the central ocean the decrease in SST is about 1°C. Once the coupled model has adjusted, however, there is very little change in the average position of isotherms over the last 20 years of integration. This is also true in other quantities monitored in the model, for example, total heat content in the ocean and atmosphere. This very small climate drift is encouraging in this coupled model. When the SST adjustment has occurred, the average SST at the western edge of the ocean is about 29°C and at the eastern edge is about 22°C. These are close to those observed in the tropical Pacific. From Fig. 1 one would deduce that the western warm pool is much too small, but Fig. 2 shows this to be somewhat misleading. Figure 2a shows the July average SST over the last 20 years of integration. It shows that the position of the 28°C isotherm on the equator is not a good indicator of the extent of the warm pool greater than 28°C. Figure 2a is typical of monthly average SSTs in the ocean and shows that the ocean model has either too much upwelling along the equator or has the water being upwelled too cold. The extent of the model warm pool is not as large as in the climatology of Shea et al. (1992) shown in Fig. 2b so that the model warm pool is slightly cold. Comparison of Figs. 2a and 2b shows that the temperature on the equator in the east is about 23°C, which is also slightly colder than the July climatology. The largest difference between the figures is that the real ocean is much colder off Baja California and South America than in the model. This is because the ocean model does not contain the mid-latitude gyres that advect colder water into these regions.

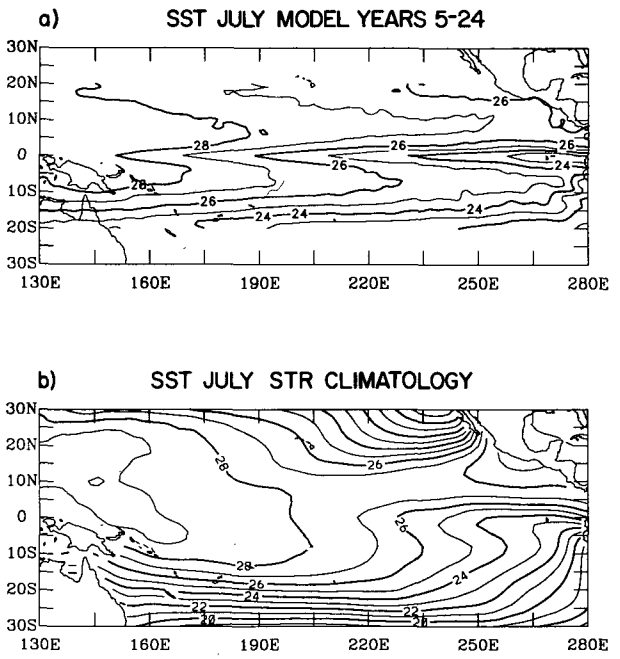

FIG. 2. (a) The July average SST over the last 20 years of the control run and (b) July SST from the Shea, Trenberth, and Reynolds climatology. In this and subsequent figures, the landmasses are shown only for reference when displaying model results.

The SST anomalies corresponding to the SST values shown in Fig. 1 have been calculated. The anomalies are not straightforward to interpret but can be grossly summarized as follows. The largest SST anomalies, which are in the eastern third of the basin, grow and decay in place and there is no clear evidence of propagation. In contrast, most of SST anomalies in the western and central thirds of the basin show clear evidence of moving to the east across the domain. This description supplants that given in Neelin et al. (1992) where the SST anomalies from an earlier version of the coupled model are described as standing and not propagating.

A comparison of monthly averaged wind stress from the FSU climatology of Legler and O'Brien (1984) and the coupled model is shown in Figs. 3 and 4 for April and October, respectively. The most obvious difference between model and observations is that the structures in both components of model stress are much more elongated zonally, which is to be expected in the aqua-planet version of CCM1. Peak values of both components of wind stress in the model and FSU data are almost the same, 1 dyn cm^{-2} in τ^x in both April and October, 0.6 and -0.6 dyn cm^{-2} in τ^y, respectively, in April and October. However, because of the elongated structures, integrated values of τ^x across the ocean are somewhat larger in the model than in the data and this may drive stronger zonal equatorial ocean currents.

The strength of the annual cycle in SST in Fig. 1 is considerably smaller than in the Pacific, especially in the eastern part of the ocean. This can be attributed to the aqua-planet version of CCM1, which takes out continentality and topography, both of which make a large contribution to the amplitude of the annual cycle in the atmosphere and, thus, to the wind stress. In addition, the interannual variability in Fig. 1 is smaller than in the Pacific, and certainly no large El Niño events occur when the central and eastern parts of the equatorial ocean warm to 28°C or 26°C, respectively. However, from year 6 or so onward the coupled model does oscillate with an amplitude of about 0.5°C in equatorial SST and a dominant period of about two years. Munnich et al. (1991) have also found 2-year oscillations in a highly simplified coupled model based on the Zebiak and Cane (1987) model. The two-year oscillation is indicative of the weak coupling regime in

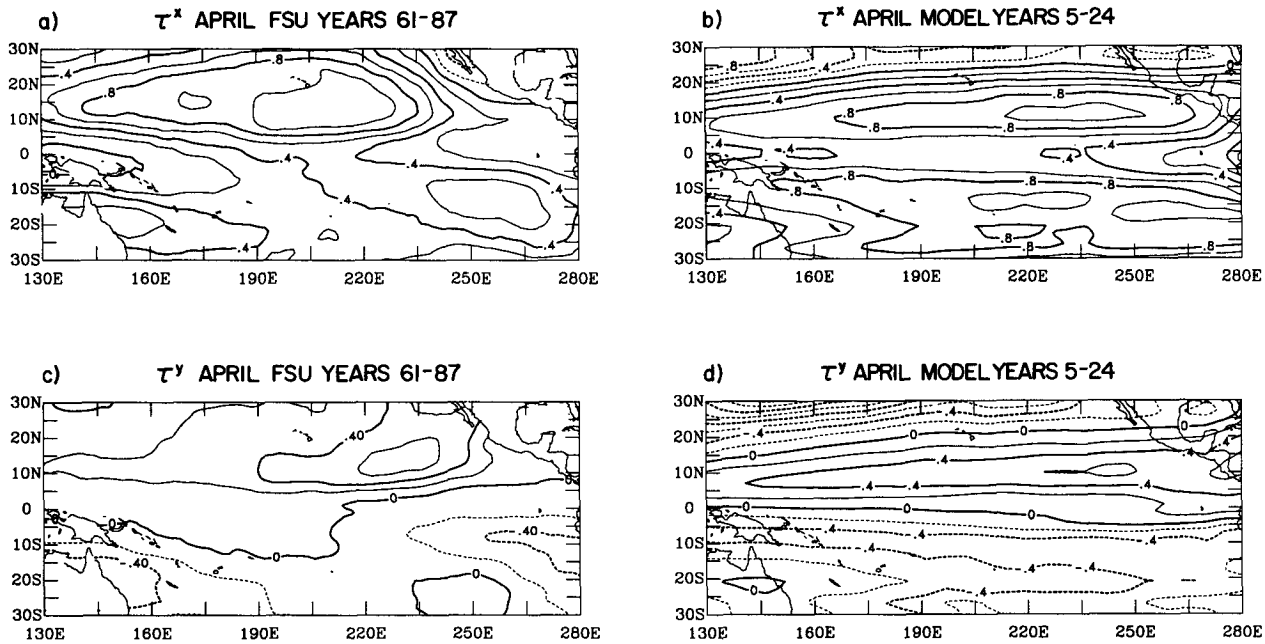

FIG. 3. Monthly averaged wind stress fields for April: (a) τ^x from FSU data, (b) τ^x from last 20 years of the control run, (c) τ^y from FSU data, and (d) τ^y from last 20 years of the control run.

the Munnich et al. work and the period of the dominant oscillation doubles to four years if the coupling between the atmosphere and ocean is strengthened. This indicates that the coupling is weak in this coupled GCM.

This is confirmed by looking at standard deviations of coupled model fields. The standard deviation of monthly averaged January SST anomalies over years 9–16 of the integration is shown in Fig. 5a and from the CAC analysis of COADS data over years 1970–1988 in Fig. 5b. The model variability is clearly smaller than natural variability. In the model the region where the standard deviation is greater than 0.5°C is considerably smaller and nowhere in the model does the standard deviation reach 1°C. The maximum values are off the equator and represent strong 20–30-day wave generation. In the COADS data the standard deviation is greater than 1°C along the equator in both the central and eastern equatorial Pacific. The ocean model has now been configured in a realistic-geometry Pacific basin and a 20-year run has been completed using The Florida State University (FSU) monthly wind-stress climatology of Legler and O'Brien (1984) to drive the model. The FSU pseudostress in $m^2\ s^{-2}$ has been converted into stress in dyn cm^{-2} by multiplying by 0.017. The standard deviation of the monthly averaged January SST anomalies from 1970–1988 is shown in Fig. 5c. The standard deviation from this ocean-alone run has the same general shape as that from observations and is slightly larger. The maximum values are greater than 1.5°C along the equator in the central Pacific. Nearly the entire ocean between 20°N and S has values greater than 0.5°C. This is in sharp contrast to the coupled-model standard deviation in Fig. 5a. Figure 6a shows the standard deviation of monthly averaged τ^x from years 9–16 of the coupled model and the same quantity from the FSU climatology for 1970–1988 is shown in Fig. 6b. Figure 7 shows the analogous plots but for τ^y. Both components of the wind stress from the coupled run have very small regions where the standard deviation is greater than 0.2 dyn cm^{-2} and it is less than 0.1 dyn cm^{-2} along the equator in both components. The FSU climatology has large areas where the standard deviation is greater than 0.2 dyn cm^{-2}. Again these differences are to be expected because of the aqua-planet version of the CCM1 being used, and the conclusion is that the atmosphere–ocean coupling in this coupled model is considerably weaker than in reality.

Figure 16 of Neelin (1990) is a schematic bifurcation diagram for his coupled model, which plots amplitude of the coupled oscillations against the relative coupling coefficient (RCC). In a series of experiments, Neelin multiplied the wind-stress anomaly that resulted from a given ocean state by the RCC. The initial ocean state was found through forcing the model by 0.42 times the wind stress of Hellerman and Rosenstein (1983). A bifurcation from stability to coupled oscillations occurred for $0.6 < RCC < 0.7$ and a further bifurcation occurred when the RCC was about 0.9. Where does the present coupled model fit in this bifurcation diagram of Neelin (1990)? In order to answer this, a teleconnectivity calculation was done first. It computes the maximum absolute values of the correlation coefficient (CC) calculated at zero lag between monthly

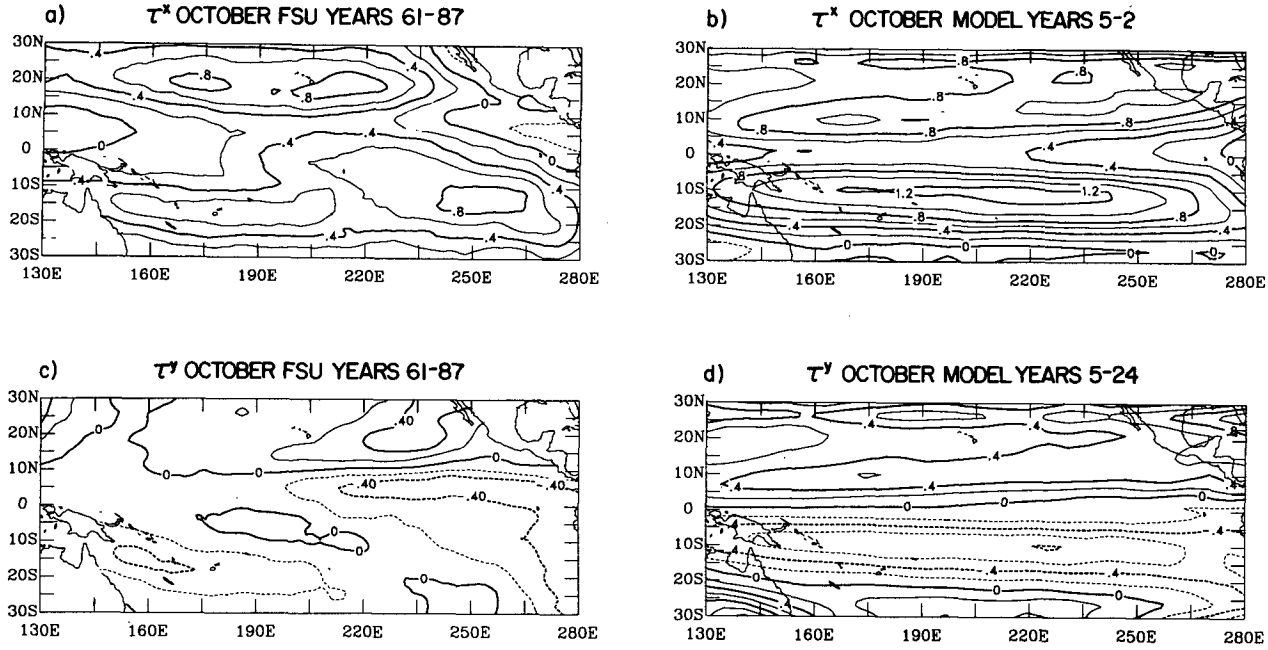

FIG. 4. Same as Fig. 3 except for October.

anomalies of SST and τ^x taken from years 9–16 of the coupled run. There are two regions where the maximum CC is larger than 0.6. Both are centered on the equator between 140° and 150°E and 180° and 155°W. The largest CC is 0.65 and occurs for SST anomalies at 2°N, 170°W. Figure 8 is a plot of the CC at zero lag between SST monthly anomalies at 170°W, 2°N and τ^x monthly anomalies over the ocean model domain. The largest CCs greater than 0.5 are found between 3° and 15° immediately to the west of 170°W. This is not very surprising because changes in τ^x generate equatorial Kelvin waves that propagate rapidly eastward, changing the SST. A first baroclinic mode Kelvin wave propagates across 15° of longitude in about 12 days, which is unresolved by the CC using monthly means. Figure 8 shows that the maximum CC is between SST at 2°N, 170°W and τ^x at 2°N, 178°W. These anomalies are plotted against each other in Fig. 9. The correlations are positive so that a reduction in the normally negative values of τ^x on the equator at the date line induces warmer SSTs at 170°W. This is consistent with the effect of Kelvin waves on SST. The correlation can also be interpreted as a positive SST anomaly at 170°W produces stronger atmospheric convection. This causes a convergence at 170°W, which implies a positive τ^x anomaly at 178°W.

A question to be addressed is, Are the τ^x and SST anomalies plotted in Fig. 9 correlated or does the spread of points reflect independent variability of the atmosphere and ocean models? It can be seen from Fig. 9 that when the τ^x anomaly is zero, the SST anomalies range between ±0.5°C. The standard deviation of this variability is 0.3°C. This value is the same as the standard deviation of SST anomalies at 2°N, 170°W in a 10-year repeating annual cycle run of the ocean model alone, forced by the averaged FSU wind-stress climatology. Similarly when the SST anomaly is zero, the τ^x anomalies range between ±0.125 dyn cm^{-2} giving a standard deviation of about 0.075 dyn cm^{-2}. Again this is consistent with the standard deviation of τ^x at 2°N, 178°W in the perpetual January run of the aquaplanet version of CCM1 with fixed SST. However, the range of τ^x and SST anomalies in Fig. 9 are ±0.2 dynes cm^{-2} and ±1°C, which are significantly larger than the independent variability of the atmosphere and ocean models. Thus Fig. 9 represents the correlated components of the τ^x and SST anomalies. The slope of a best-fit line to the data in Fig. 9 would show that a 1°C SST anomaly is consistent with a 0.2 dyn cm^{-2} anomaly in τ^x. This is a reasonable size anomaly in τ^x for a 1°C SST anomaly when compared to what Neelin (1990) found using anomalies during El Niño events. However, in the El Niño events the SST anomalies were often 2°C and sometimes 3°C, whereas most of the SST anomalies from this coupled model are less than 0.6°C. Thus the coupled model is unable to produce realistically large anomalies, but the relative size of anomalies in SST and τ^x is not that far from reality.

Figure 10 is a schematic extension of Neelin's (1990) diagram into three dimensions where the third axis is the fraction of the Hellerman and Rosenstein (1983) wind stress used to find the mean state of the ocean. Neelin's curve is reproduced when the fraction is 0.42 and the fraction estimated for the wind stress from the coupled model shown in Figs. 3 and 4 is 1. The coupled model has an RCC equal to 1 and produces coupled

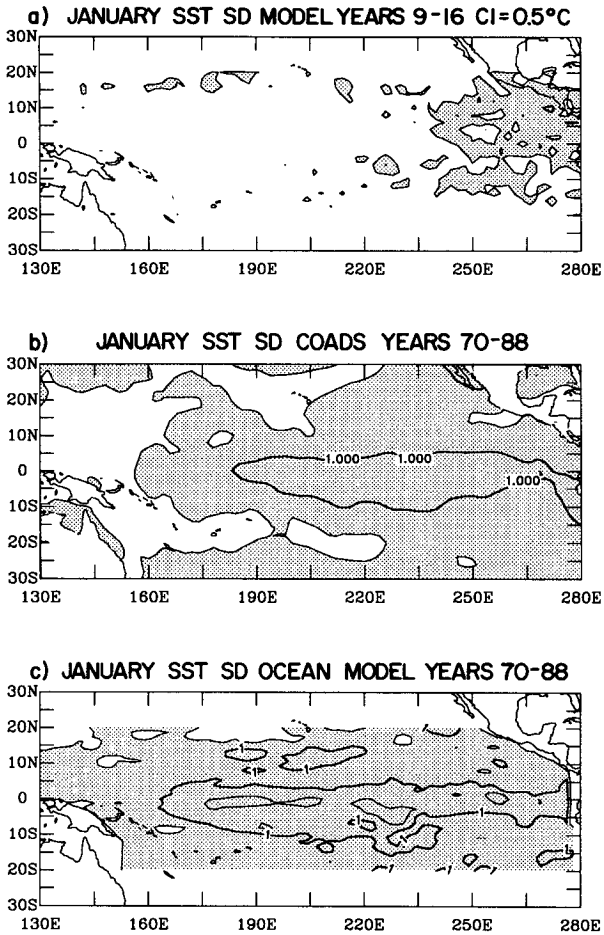

FIG. 5. Standard deviation of monthly January SST averages: (a) model from years 9–16, (b) CAC analysis of COADS data from 1970–1988, and (c) ocean model alone from 1970–1988.

oscillations so that it is probably just below the first bifurcation in the Neelin diagram. Figure 10 agrees with Neelin's conclusion that the stronger the wind stress, and, hence, circulation pattern in the ocean, the harder it is for the coupled model to have self-sustained coupled oscillations. The more interesting and exotic coupled-model behavior occurs when the mean ocean circulation is weaker than reality.

In order to examine the spatial pattern of the interannual variability in the coupled simulations, an empirical orthogonal function (EOF) analysis of the SST and wind stress anomalies was performed. Three-month running averages of the monthly anomalies were used for this EOF analysis. The first EOF of SST anomalies over years 9–16 of the coupled run is shown in Fig. 11a and the first EOF from the CAC analysis of COADS data over years 1970–1988 is shown in Fig. 11b. Figure 11c shows the first EOF of monthly SST anomalies for 1970–1988 from the ocean model with realistic geometry forced by the FSU wind-stress climatology that was described earlier. The coupled model

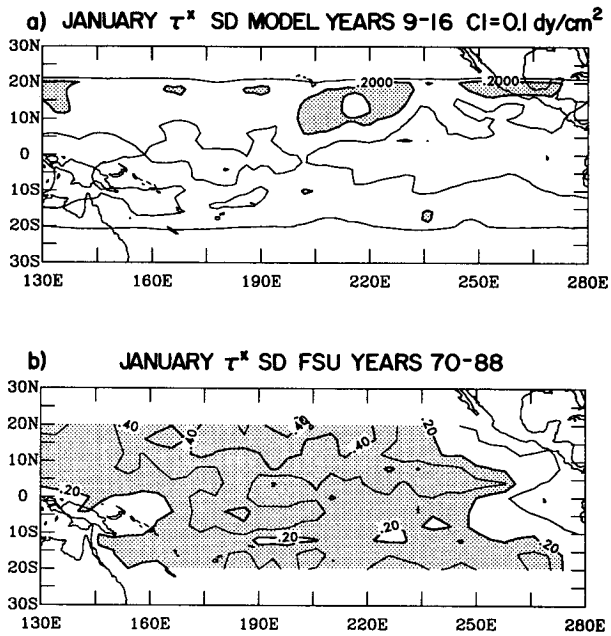

FIG. 6. Standard deviation of monthly January τ^x averages: (a) model from years 9–16 and (b) FSU analysis of data from 1970–1988.

EOF has a maximum value of 1 so that its coefficient has units of degrees Celsius, and the other two EOFs are normalized so that all EOFs have the same spatial norm. The coupled model EOF has its maximum on the eastern boundary at 8°N but also has a secondary

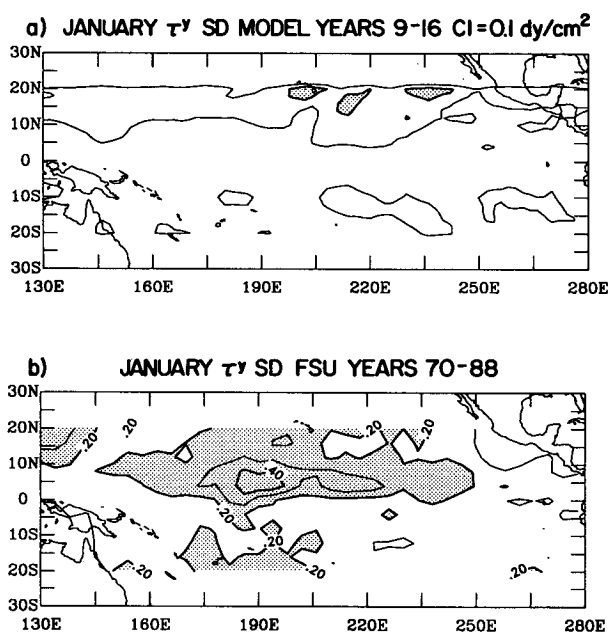

FIG. 7. Standard deviation of monthly January τ^y averages: (a) model from years 9–16 and (b) FSU analysis of data from 1970–1988.

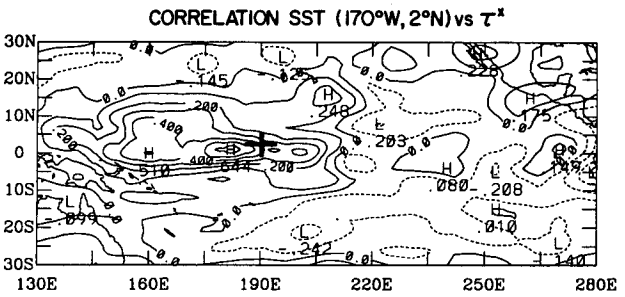

FIG. 8. Correlation map of SST monthly anomalies at 2°N, 170°W and τ^x monthly anomalies.

maximum on the equator in the eastern Pacific which is just to the east of the maximum in the EOF from COADS data. The COADS EOF has large values in the central Pacific, which is where the EOF from the ocean-model-alone run also has its largest values. These EOF patterns could be foreseen by the comparison of January SST standard deviations shown in Fig. 5. The first EOFs shown in Fig. 11 explain 24%, 58%, and 23% of the variance in the respective datasets. The larger percentage explained in the COADS data is to be expected because of the heavy spatial smoothing used in this dataset. In all three cases the variance of the second EOF is at least a factor of two smaller than the variance explained by the first EOF. The coefficient of the first coupled model EOF is plotted against time in Fig. 12, which shows that the EOF has a quite regular 2-year period over years 9–16 in the coupled integration.

The first EOFs for τ^x and τ^y from years 9–16 of the coupled run are shown in Figs. 13a and 14a, respectively. Figures 13b and 14b show the corresponding EOFs calculated from 3-month running means of the monthly averaged anomalies from the FSU climatology for 1970–1988. The FSU EOFs have been normalized so they have the same spatial norm as the model EOFs. The first EOFs of τ^x explain 24% and 16% of the variance in the model and FSU climatology, respectively, and those of τ^y explain 25% and 23%, respectively. Figure 13 shows that the coupled model does not exhibit the variability in τ^x that is centered on the equator at the date line in reality. In the coupled model the variance in τ^x is maximum off the equator in the west and east Pacific. This is probably the most important reason why the coupled model variability is not like ENSO variability. Figure 14 shows that the coupled-model variability in τ^y is much more like that in the FSU climatology. Both have maximum values off the equator to the north and south, but the maximum variability in the model is somewhat to the west of that in reality. In both the coupled model and the FSU climatology, the second EOF of τ^y explains a considerably smaller percentage of the variance than the first, and the time series of the first EOF in τ^y is highly correlated with the time series of the first EOF in SST. This is not so true for τ^x, however. In both the model and FSU data the second EOF of τ^x explains only a somewhat smaller percentage of the variance than the first EOF. In the FSU data, when the 3-month running average has been applied, the time series of the first EOF in τ^x correlates quite well with that of the first EOF of SST data. However, in the coupled model the time series of the first EOF in τ^x is only correlated moderately well with that of the first EOF of SST shown in Fig. 12. The second model EOF of τ^x contributes significantly to the variability of the first SST EOF.

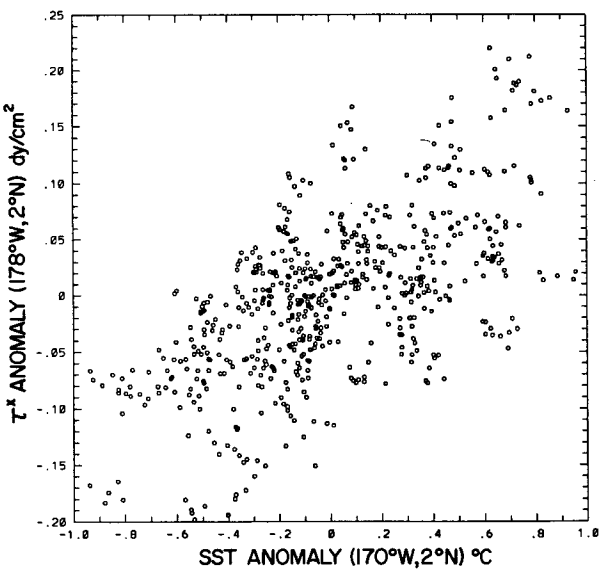

FIG. 9. Plot of τ^x monthly anomalies at 2°N, 178°W against SST monthly anomalies at 2°N, 170°W.

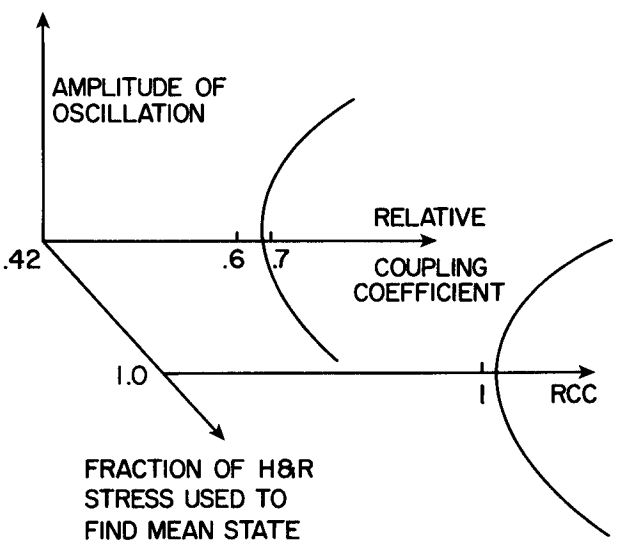

FIG. 10. Schematic bifurcation diagram from Neelin (1990). See text for details.

In summary, the coupled-model oscillations have several features that are characteristic of ENSO behavior, but their amplitudes are weak, their spatial extent is a little small, and their period is regular and too short.

4. Model-twin experiments

The model-twin experiments were performed by making a very small perturbation to the ocean temperature distribution at a particular time in the long control integration and then integrating the coupled model for a year or so. The reason to perturb only SST is that it evolves on the slow ocean time scale and is the only ocean variable important to the atmosphere. This was thought to be more appropriate for these coupled-model experiments than making initial perturbations to atmospheric variables. A pattern correlation coefficient between the monthly SST anomalies in each model-twin experiment was calculated using 7500 points from the whole 150° of longitude (150 points) and between 15°S and 15°N (50 points). The same mean monthly SST values were subtracted from all twin integrations, namely, the mean from years 9–16 of the control integration. The initial temperature perturbation had a maximum amplitude of 10^{-4} °C and its spatial pattern was that of the first SST EOF shown in Fig. 11a. The vertical profile of the temperature perturbation used at each horizontal location was that of the long-term average temperature profile at that location. This initial change is very small, but some experiments with a larger initial change of 10^{-1} °C were run and are also described.

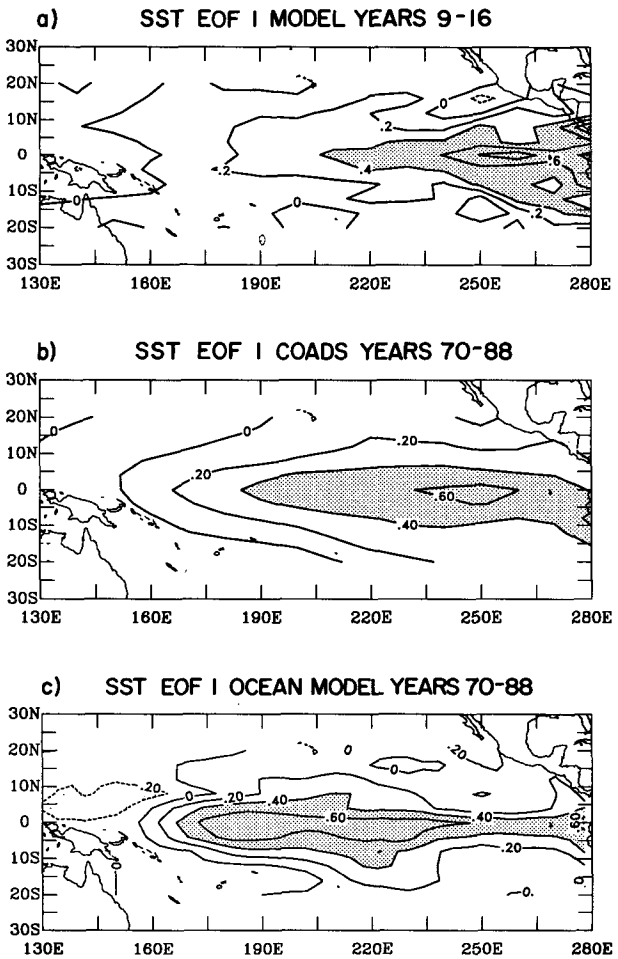

FIG. 11. Spatial pattern of first EOF of monthly SST anomalies: (a) model from years 9–16, (b) CAC analysis of COADS data from 1970–1988, and (c) ocean model alone from 1970–1988.

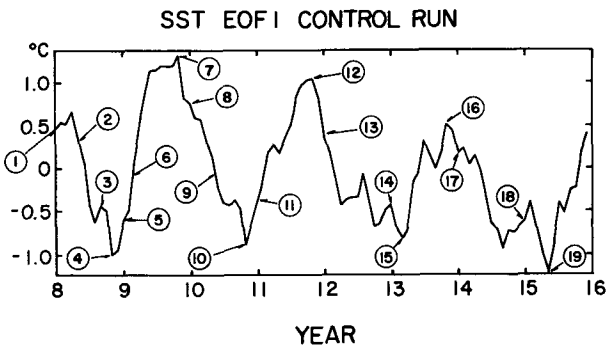

FIG. 12. Plot of coefficient of first EOF of monthly SST anomalies versus time for years 9–16 of the control run. The circled numbers indicate the start of the 19 model-twin experiments.

A total of 19 model-twin experiments were carried out and the times of the initial perturbation are shown in Fig. 12. Figure 15 is a plot of the correlation coefficient for the ensemble mean of all 19 experiments versus time. The model-twin experiments decorrelate quite quickly with the correlation coefficient dropping to 0.5 after 4.5 months and to 0.2 after 12 months. The mean plus and minus the standard deviation of the 19 cases is also plotted in Fig. 15 and shows that the time to decorrelate to 0.5 ranges between 3.5 and 5.5 months and the correlation coefficient ranges between 0.07 and 0.33 after 12 months. The standard deviation has been calculated using the Fisher z transform. These decorrelation times are quite short, although the test is stringent in the sense that the model is being asked to get the correct SSTs at 7500 grid points. The predictability times in this study may also be a lower limit because the spatial pattern of the SST perturbation is not random but is the first EOF pattern, which by definition varies the most in the control integration.

The decorrelation times in Fig. 15 are nonetheless surprisingly short given that the maximum initial SST perturbation is 10^{-4} °C. This perturbation increases rapidly in size and Fig. 16a shows that maxima monthly averaged SST differences between case 1 model-twin experiments are greater than 1°C in March when the initial perturbation was made on January 1. The max-

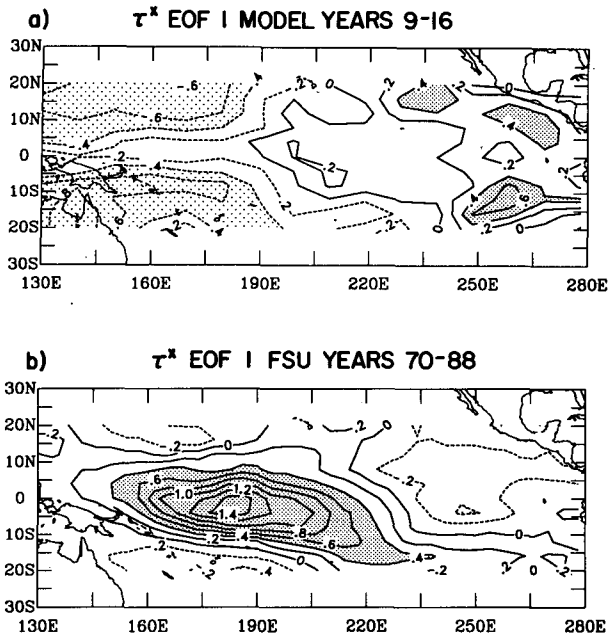

FIG. 13. Spatial pattern of first EOF of monthly τ^x anomalies: (a) model from years 9–16 and (b) FSU analysis of data from 1970–1988.

ima are on the equator in the eastern part of the basin, which is near the maximum initial perturbation (see Fig. 11a). The SST differences both increase in size in the eastern part of the basin and appear elsewhere in the basin by June, (see Fig. 16b) but do not increase further, so that the SST differences in September are still mostly less than 1°C, see Fig. 16c. This is consistent with the SST standard deviation of 0.5°C shown in Fig. 5a.

In the initial stages of this model-twin experiment, the SST differences increase from 10^{-4} °C to 10^{-1} °C in about two weeks. This means that the decorrelation times of monthly averages should not be greatly different if the initial perturbation amplitude is 10^{-4} °C or 10^{-1} °C. This is confirmed by the results shown in Fig. 17. Cases 1 and 5 were repeated using an initial perturbation amplitude of 10^{-1} °C. The pattern correlation coefficients from these four experiments are plotted versus time in Fig. 17. Figure 17a shows there is almost no change in decorrelation time when the correlation coefficient drops more rapidly than the ensemble mean. Figure 17b shows that the larger-initial-amplitude case does decorrelate a little more quickly when the correlation coefficient drops less quickly than the ensemble mean. Thus, the decorrelation times are relatively insensitive to the amplitude of the initial perturbation up to 10^{-1} °C changes, which is about 20% of the SST standard deviation shown in Fig. 5a.

In previous studies of ENSO predictability the simpler Zebiak and Cane (1987) model was asked only to get the correct SST in the large NINO3 area (5°S to 5°N and 90°W to 150°W). Therefore, it could be argued that the short decorrelation times in this model are a result of too stringent a criteria being applied. Perhaps the decorrelation times would be longer if only one number or coefficient were to be predicted. Initially the coefficient of the first SST EOF calculated from years 9–16 in the control integration was used. The coefficients of this EOF for four model-twin experiments are plotted versus time in Fig. 18. The four experiments are cases 1 and 5 with initial SST perturbation amplitudes of 10^{-4} °C and 10^{-1} °C. Thus the coefficient from the control run shown in Fig. 18 is exactly the same as in Fig. 12 but on a shorter time scale. Figure 18 shows that the predictability times may be longer when predicting the first EOF coefficient rather than the total SST variability. This is confirmed by the results shown in Fig. 19. It shows the correlation coefficient between the 19 model-twin experiments versus time when predicting either the coefficient of the first EOF or the NINO3 SST. The plots are similar and most of the predictability is lost over the first 6 months, but then the predictability recovers to significant values at 8 months and longer. This contrasts with the predictability of total SST variability shown in Fig. 15, which is a monotonically decreasing function of time over the first year. However, the rapid loss of predictability over 6 months is a characteristic of this coupled model and depends only slightly on the verification measure.

Figure 18 also shows that the prediction of the first EOF coefficient is better for a longer time in case 5

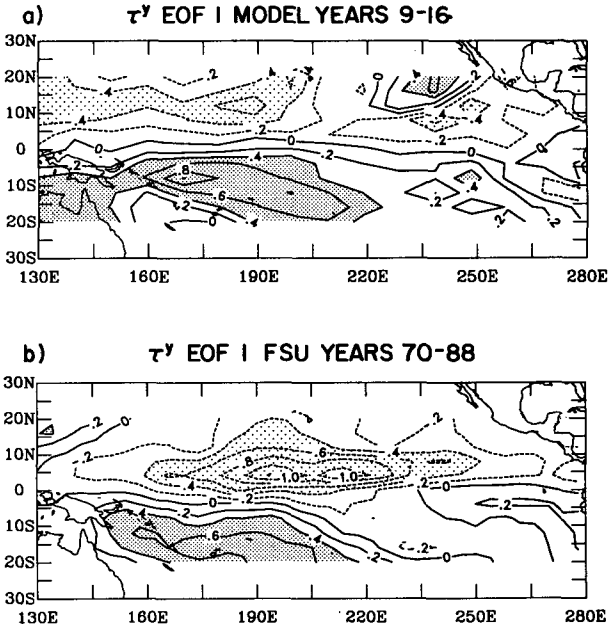

FIG. 14. Spatial pattern of first EOF of monthly τ^y anomalies: (a) model from years 9–16 and (b) FSU analysis of data from 1970–1988.

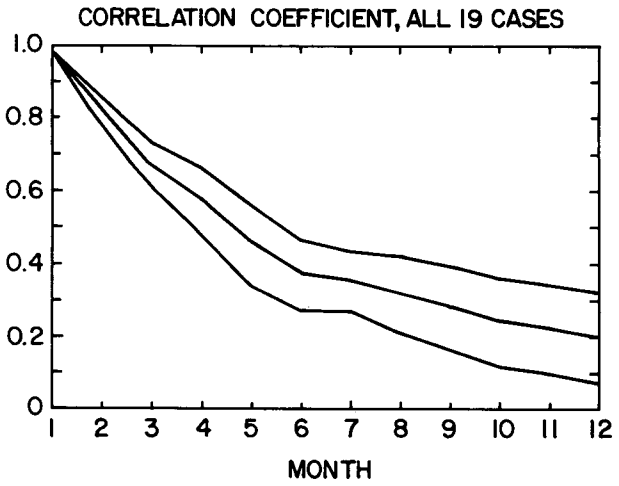

FIG. 15. Correlation coefficient calculated between 15°S and 15°N over the whole domain versus time for the mean and mean plus and minus the standard deviation of all 19 model-twin experiments.

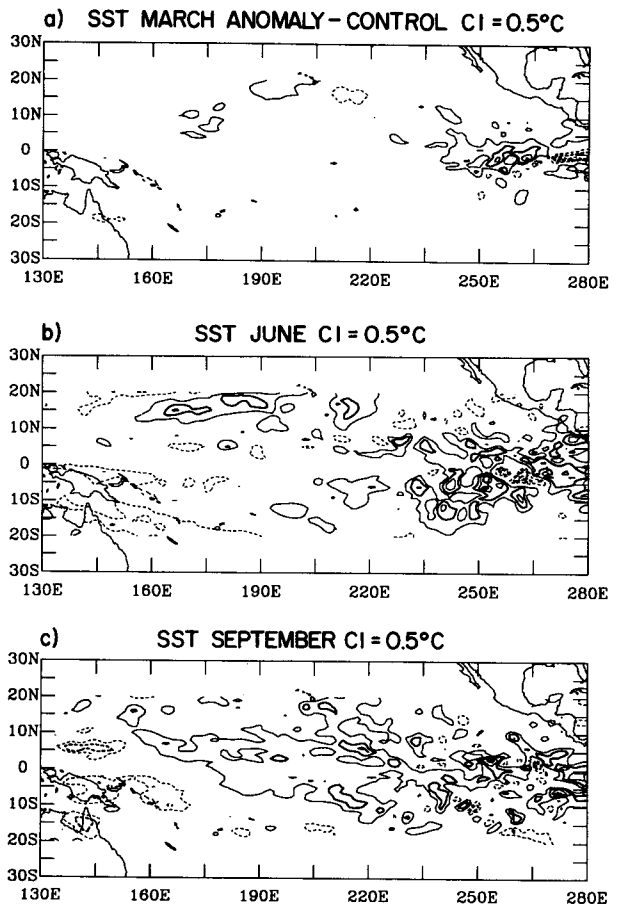

FIG. 16. Monthly averaged SST differences anomaly minus control for case 1 (10^{-4} °C change at 1 January, year 9): (a) March, year 9; (b) June, year 9; and (c) September, year 9. The zero contour is not shown and negative contours are dashed.

than in case 1. Thus, a hypothesis may be made that the predictability times in this coupled model are longer when predicting the onset of a warm event (case 5, for example) than when predicting the onset of a cold event (case 1, for example). This hypothesis was tested by dividing most of the model-twin experiments into two sets. Cases 4, 5, 6, 10, 11, 15, and 19 attempt to predict the onset of a warm event, whereas cases 1, 2, 7, 8, 12, 13, 16, and 17 attempt to predict the onset of a cold event. The ensemble mean pattern correlation coefficients of these two sets are plotted against time in Fig. 20. There is very little difference between the two sets over the first 6 months when both decorrelate to less than 0.4, but at longer times, up to 12 months the correlation is higher when predicting a warm event rather than a cold event. This difference is significant at one year where the mean minus standard deviation of the warm events equals the mean plus standard deviation of the cold events. Thus there is some support for the hypothesis that in this coupled model it is easier to predict a warm event 6 to 12 months ahead than it is to predict a cold event.

5. Diagnosis of a model-twin experiment

In this section the case 1 model-twin experiment is diagnosed in more detail to see why and how the two

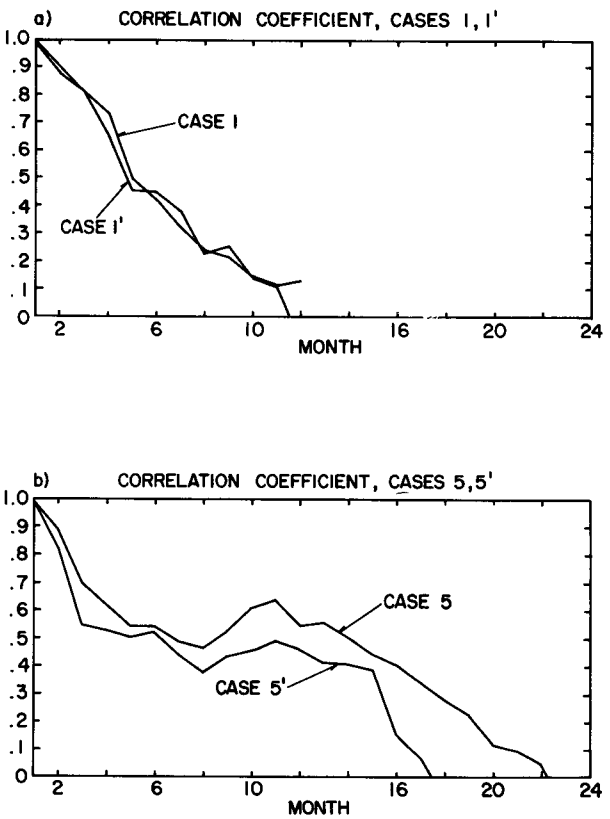

FIG. 17. Correlation coefficient versus time for initial changes of 10^{-1} and 10^{-4} °C: (a) case 1 and (b) case 5.

integrations diverge. Daily averages of differences between anomaly and control run quantities were examined in order to see which quantity showed the first significant change and when. These quantities included all components of the heat flux and wind stress produced by the atmosphere and all terms that contribute to the SST balance in the ocean. The first variable to show a significant change was the incoming shortwave radiation at the surface on day 6 after the initial 10^{-4} °C change in SST. The daily average difference between the anomaly and control runs at day 6 of shortwave radiation is shown in Fig. 21c, which shows many small areas where the radiation difference is up to 50 W m^{-2}. Figure 21b shows the difference in the clouds between the two integrations at day 6. It is clear that the changes in solar radiation are due solely to changes in the amount of cloud through Eq. (2). The tropical troposphere is nearly always close to saturation so that very small changes in SST can induce small changes in the static stability that then cause changes in the amount of cloud. The cloudiness then changes the solar radiation by up to 50 W m^{-2}. These changes in SST, shown in Fig. 21a, and static stability also cause much smaller changes in the other components of the heat flux, whose maximum differences are about 10 W m^{-2}, and in the wind stress. The changes in wind stress and total heat flux between the two integrations at day 6 are shown in Fig. 22. The maximum changes in τ^x and τ^y are of the order of 0.02 and 0.006 dyn cm^{-2}, respectively, and Fig. 22c shows that the changes in total heat flux are almost all due to the change in incoming solar radiation. These differences in the forcing fields then produce differences in the ocean circulation and SST, but the initial changes in SST are mainly caused by the change in heat flux. By day 15 the changes in the coupled system start to become significant and the two integrations diverge.

The first question to be addressed is, Are the changes in solar radiation of 50 W m^{-2} 6 days after a change in SST on the order of 10^{-4} °C reasonable or too large due to the simple parameterization of radiation used? In order to answer this question, two integrations of CCM1 with the full radiation calculation were performed using the evolving SSTs from the control and anomaly runs. These integrations show that differences in the incoming solar and total heat fluxes in some locations of 50 W m^{-2} after 6 days are consistent with the full radiation calculation in the model.

The second question is, Would the decorrelation time in the model-twin experiment be much longer without the cloud feedback on solar radiation? In order to answer this the model-twin experiment was repeated but with the incoming solar radiation held constant in time at its initial value in both runs. In this model-twin experiment, differences do not start to appear until day 12, and they first appear in the evaporative and sensible heat fluxes. The daily average difference at day 12 of SST, evaporative, and sensible heat fluxes between the anomaly and control runs are shown in Fig. 23 and those of τ^x, τ^y, and total heat flux are shown in Fig. 24. Comparison of Figs. 22 and 24 shows that, in the case with no cloud feedback, the changes in wind stress are larger but the change in heat flux is the same order of magnitude. In this case the initial changes in SST

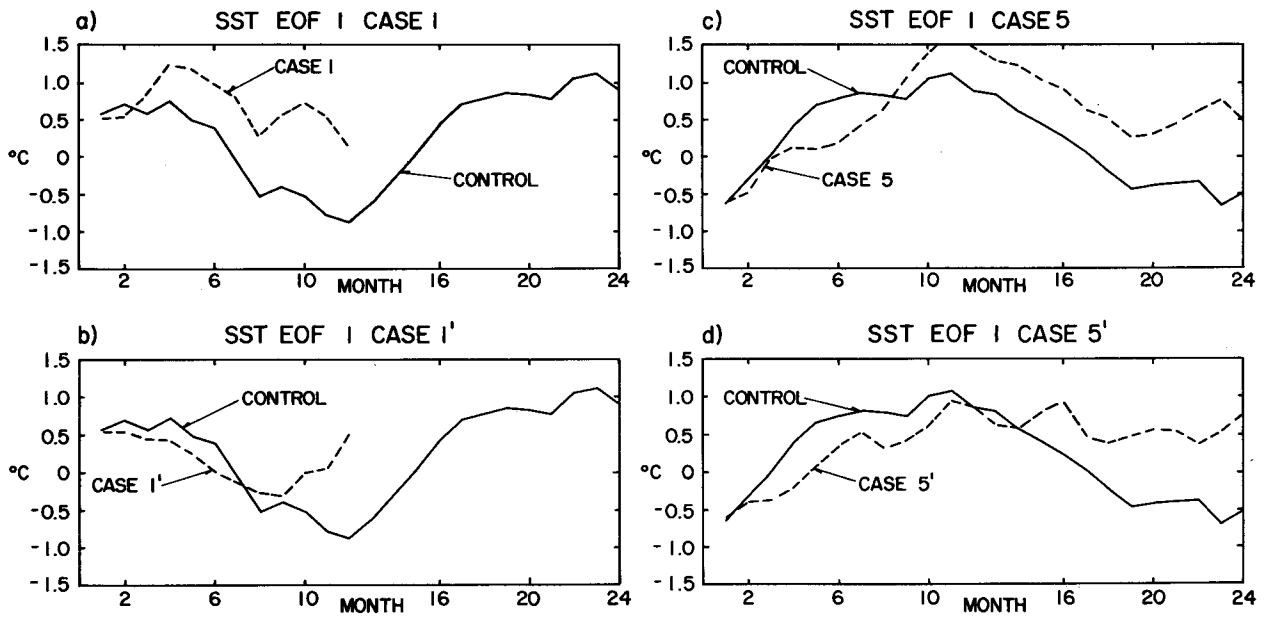

FIG. 18. Coefficient of first EOF of monthly SST anomalies versus time in model-twin experiments: (a) case 1, (b) case 1′ (10^{-1} °C initial change), (c) case 5, and (d) case 5′ (10^{-1} °C initial change).

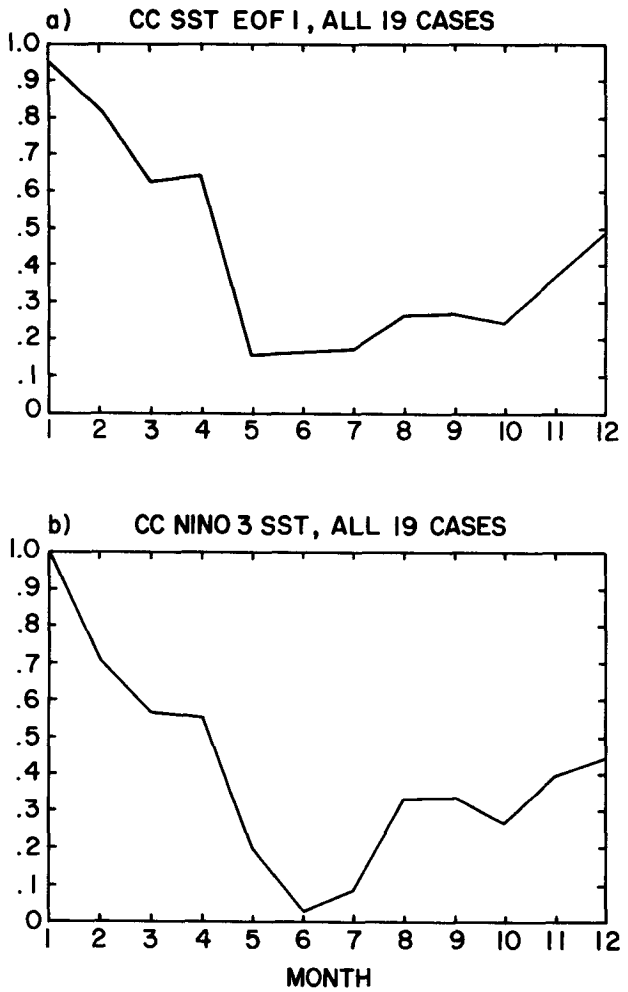

FIG. 19. Correlation coefficient versus time of all 19 model-twin experiments for (a) amplitude of first EOF and (b) NINO3 SST anomaly.

are caused both by heat flux and by advection forced by the changed wind stress. However, it is clear that the decorrelation time in model-twin experiments is not significantly longer without the cloud feedback on solar radiation.

The dynamical feedback described above is not an artifact of an overactive aqua-planet version of the atmospheric GCM. The kinetic energy of transient disturbances in the tropical belt of the aqua-planet model gives a root-mean-square velocity magnitude of about 5 m s^{-1}, which is close to, although somewhat smaller than, the value from observations. Thus, as far as synoptic time-scale phenomena are concerned, the magnitude of forcing from the atmospheric component of the coupled model is not excessive.

The divergence of the other model-twin experiments is almost certainly similar to that described above for case 1. A similar divergence of model-twin experiments would also almost certainly occur if the initial perturbation was made in atmospheric variables rather than in SST. This suggests that many detailed features of the tropical coupled ocean–atmosphere system are not predictable very far ahead of time.

6. Discussion and conclusions

The simulation described in section 3 has its successes and failures. The coupled model does have sustained oscillations that are caused by the instability of the coupled ocean–atmosphere system. The first EOF of monthly SST anomalies shown in Fig. 11a is completely different from the equivalent quantity calculated from a run of the ocean model alone forced by a repeating annual cycle of wind stress from the FSU climatology. However, Fig. 11b shows that the model EOF is not very close to the EOF from COADS data. The comparison of January SST standard deviation from the model and COADS data in Fig. 5 also shows

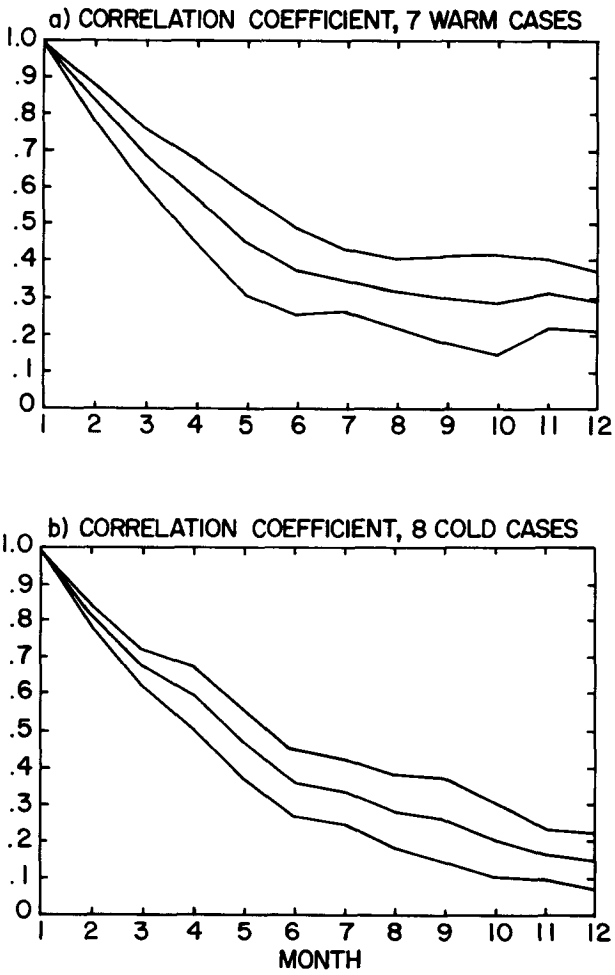

FIG. 20. Correlation coefficient versus time for the mean and mean plus and minus the standard deviation of (a) 7 cases predicting a warm event and (b) 8 cases predicting a cold event.

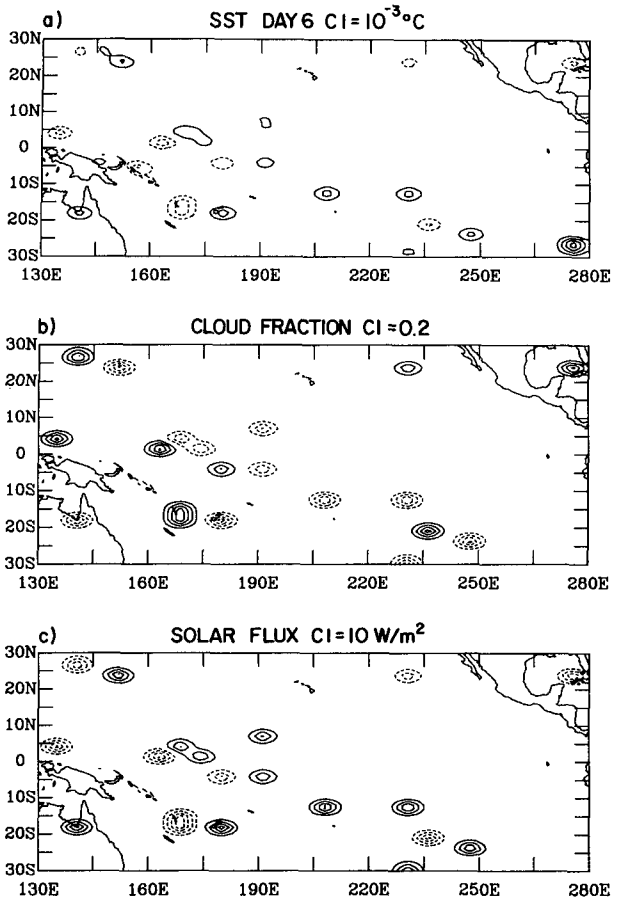

FIG. 21. Differences between anomaly minus control 6 days after initialization of model-twin experiment 1: (a) SST, (b) cloud fraction, and (c) incoming solar flux at the surface.

that the coupled model does not do very well. The successes of the model integration shown in Fig. 1 are the small climate drift and good mean values of the SST along the equator. The failures are the small amplitudes of annual and interannual variability deduced from Fig. 1.

What is the reason for this small variability? One possibility is weaknesses in the atmospheric model and the ocean model not associated with the aqua-planet and rectangular basin versions of these models. The atmospheric model is known to have relatively poor parameterizations of the planetary boundary layer and convection. It is clear from Fig. 13 that the first EOF of τ^x in the coupled model is very different from the first EOF from the FSU climatology. The ocean model contains no explicit mixed-layer physics and the shielding of the deep ocean from high-frequency changes in the forcing is crudely parameterized by averaging the forcing fields over the previous week. Perhaps changes in the ocean model forcing do not produce large enough changes in SST. This question is addressed by Fig. 9, which is a plot of anomalies of τ^x at 2°N, 178°W against anomalies of SST at 2°N, 170°W. The slope of a best-fit straight line to the points would indicate that a SST anomaly of 1°C produces an anomaly in τ^x of 0.2 dynes cm^{-2} and vice versa. This slope is in agreement with Neelin's (1990) analysis using anomalies during El Niño events. Thus, one of the conclusions of this work is that the small annual and interannual variability in this coupled model is mostly due to the aqua-planet approximation made to CCM1. This approximation eliminates land–sea contrasts, strong standing waves, and the Asian monsoon. The simplification of the ocean model from realistic geometry to a rectangular basin is not thought to reduce the coupled-model variability. This is based on simulations of the 1982–83 El Niño using the analyzed FSU winds. The simulations were not very different in rectangular and realistic geometry basin versions of the ocean model. Thus the weakness of variability in this system is likely a reflection of the amplitude of interannual fluctuations to be expected in an aqua-planet model.

The model-twin experiments described in section 4 show that when a very small change is made to the

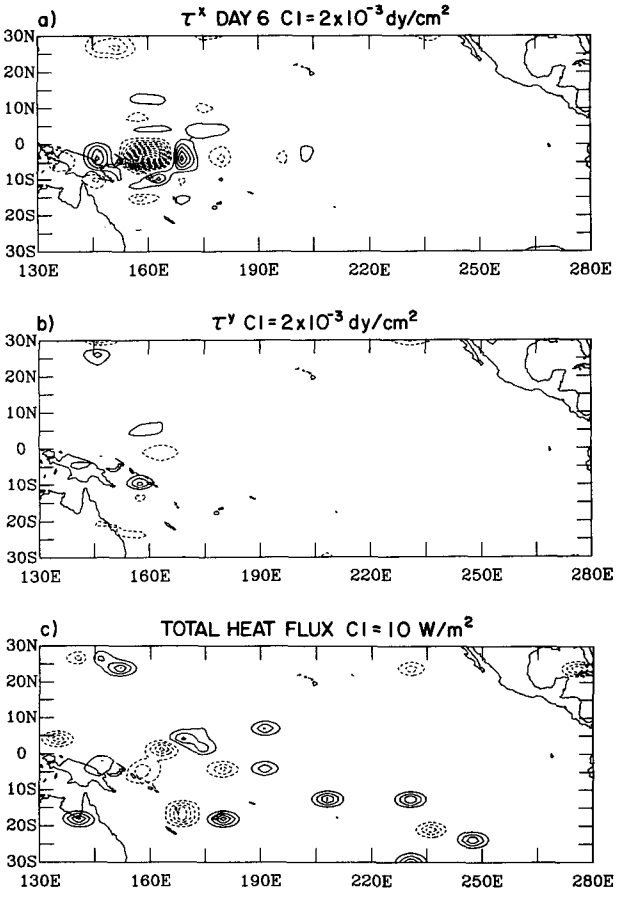

FIG. 22. Same as Fig. 21 but for (a) τ^x, (b) τ^y, and (c) total heat flux at the surface.

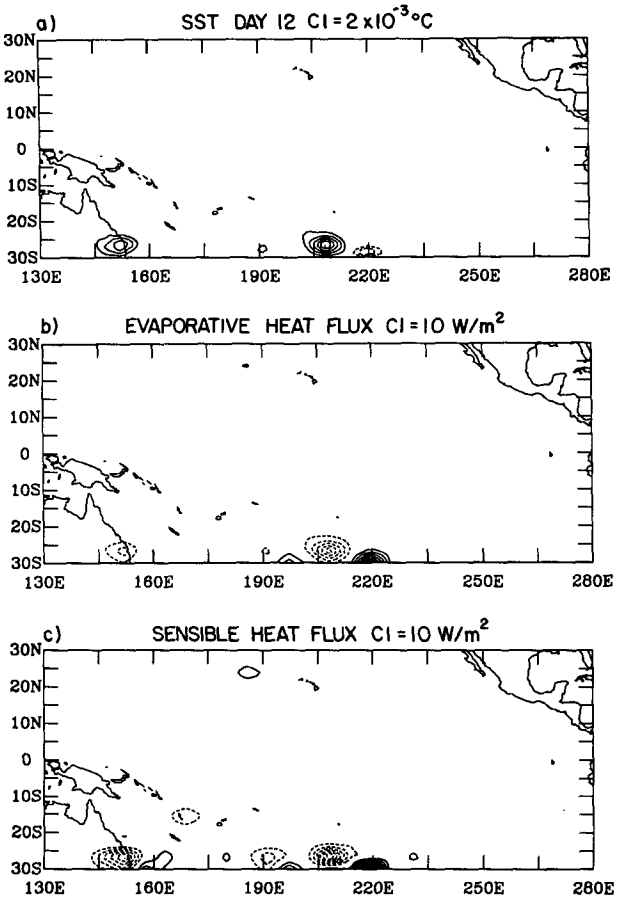

FIG. 23. Differences between anomaly minus control 12 days after initialization of case 1 but with no cloud feedback: (a) SST, (b) evaporative heat flux, and (c) sensible heat flux.

SST field, integrations of the coupled model diverge quite rapidly. Figure 15 shows that the ensemble mean pattern correlation coefficient drops to 0.5 after 4.5 months. This fast decrease in correlation coefficient indicates that the model-twin experiments diverge in the details of their SST fields in 6 months and the analysis in section 5 shows that this is initially due to changes in the cloud fraction that cause changes in the incoming solar radiation. These changes occur after about 6 days, which is about the predictability time found from studies of atmospheric GCMs alone. The predictability is only marginally improved by using the coefficient of the first SST EOF or NINO3 SST as the sole predictor. Figure 19 shows that predicting these single numbers in this coupled model at times shorter than 6 months is no better than predicting the total SST variability. Figure 20 shows that predicting a warm event may be somewhat easier than predicting a cold event.

Figure 15 shows that the ensemble mean pattern correlation coefficient drops more slowly between 6 and 12 months. This behavior is reminiscent of that found by Goswami and Shukla (1991) for model-twin experiments with the Zebiak and Cane (1987) model. Their Fig. 10b shows two rates of error growth but the break between them is at two years rather than at 6 months as in Fig. 15. Blumenthal (1991) gives an elegant explanation for the two time scales in the Goswami and Shukla study. The large initial growth rate is found because the coupled system is not self-adjoint. In such a system there is the possibility of error growth in a mode completely unrelated to the fastest-growing linearly unstable mode.

Graham et al. (1992) performed predictability studies with the Zebiak and Cane (1987) model, which consisted of model-twin experiments and comparison of the model NINO3 SST predictions with observations. In their model-twin experiments the correlation coefficient based on 288 cases falls to below 0.5 in the first 6 months, but then decreases much less quickly. This should be compared to Fig. 19b where the correlation in this coupled model falls to close to zero in the first 6 months. However, when the comparison is made with observations, the correlation coefficient starts between 0.6 and 0.7 at month 1, but then remains

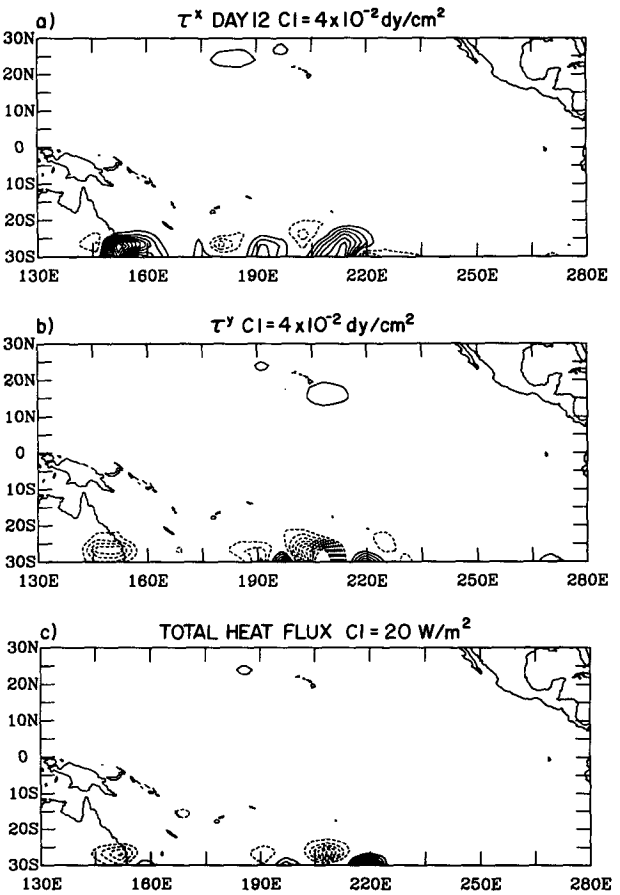

FIG. 24. Same as Fig. 23 but for (a) τ^x, (b) τ^y, and (c) total heat flux at the surface.

almost flat and is still greater than 0.5 at 12 months lead time. Thus, at lead times of greater than 4 months, the correlation with observed NINO3 SST is larger than in the model-twin experiments. In Zebiak (1989) noise was added to the zonal wind stress in the Zebiak and Cane (1987) model which simulated the noise of the 30–60-day oscillation. The addition of quite-large-amplitude perturbations to τ^x had a rather small effect on the prediction of NINO3 SST in the Zebiak and Cane coupled model.

In summary, we believe that the rapid decrease in correlation over the first few months in the model-twin experiments with this coupled model represents a real process in the tropical atmosphere. The atmosphere has independent variability that is not predictable very far ahead in time. This can lead to coupled instabilities on scales smaller than is possible in the Zebiak and Cane (1987) model. The fact that the correlations in this model rapidly decrease to much less than 0.5 is a consequence of the weak coupled oscillations. Because of this independent variability, this coupled model decorrelates on a fast time scale in a manner consistent with the fast error growth noted by Goswami and Shukla (1991), Blumenthal (1991), and Graham et al. (1992), without explicitly exciting the modes documented by Blumenthal. Rather, synoptic-scale variability in the tropical atmosphere couples with SST on the same scale, which quite quickly contaminates the large-scale features of SST represented by the first EOF. Because of this rapid error growth, we believe that making predictions of ENSO with a slave atmospheric model is the correct thing to do until the more physically complete models achieve much more realistic, strong coupled oscillations that mimic ENSO so that they can achieve the same long-term predictive skill.

Acknowledgments. Brian Kauffman and Jeff Lee coupled the two component models for this study and produced all the runs and analysis of the experiments. During this time they were supported by the NOAA Office of Global Programs through Grant NA88AANRG0140. The authors were supported by the National Science Foundation through its funding of the National Center for Atmospheric Research.

REFERENCES

Blumenthal, M. B., 1991: Predictability of a coupled ocean–atmosphere model. *J. Climate,* **4,** 766–784.

Cane, M. A., S. E. Zebiak, and S. C. Dolan, 1986: Experimental forecasts of El Niño. *Nature,* **321,** 827–832.

Gent, P. R., 1991: The heat budget of the TOGA-COARE domain in an ocean model. *J. Geophys. Res.,* **96,** 3323–3330.

——, and M. A. Cane, 1989: A reduced gravity, primitive equation model of the upper equatorial ocean. *J. Comput. Phys.,* **81,** 444–480.

Goswami, B. N., and J. Shukla, 1991: Predictability of a coupled ocean–atmosphere model. *J. Climate,* **4,** 3–22.

Graham, N. E., T. P. Barnett, and M. Latif, 1992. Considerations of the predictability of ENSO with a low-order coupled model. *TOGA Notes,* **7,** 11–15.

Hellerman, S., and M. Rosenstein, 1983: Normal monthly wind stress over the world ocean with error estimates. *J. Phys. Oceanogr.,* **13,** 1093–1104.

Legler, D. M., and J. J. O'Brien, 1984: *Atlas of Tropical Pacific Wind Stress Climatology 1971–1980.* The Florida State University Press, 182 pp.

Munnich, M., M. A. Cane, and S. E. Zebiak, 1991. A study of self-excited oscillations of the tropical ocean–atmosphere system. Part II: Nonlinear cases. *J. Atmos. Sci.,* **48,** 1238–1248.

Neelin, J. D., 1990: A hybrid coupled general circulation model for El Niño studies. *J. Atmos. Sci.,* **47,** 674–693.

——, et al., 1992: Tropical air–sea interaction in general circulation models. *Climate Dyn.,* **7,** 73–104.

Pacanowski, R. C., and S. G. H. Philander, 1981: Parameterization of vertical mixing in numerical models of tropical oceans. *J. Phys. Oceanogr.,* **11,** 1443–1451.

Shea, D. J., K. E. Trenberth, and R. W. Reynolds, 1992: A global monthly sea surface temperature climatology. *J. Climate,* **5,** 987–1001.

Williamson, D. L., J. T. Kiehl, V. Ramanathan, R. E. Dickinson, and J. J. Hack, 1987: Description of NCAR community climate model (CCM1). NCAR Tech. Note 285, 112 pp.

Zebiak, S. E., 1989: On the 30–60-day oscillation and the prediction of El Niño. *J. Climate,* **2,** 1381–1387.

——, and M. A. Cane, 1987: A model El Niño/Southern Oscillation. *Mon. Wea. Rev.,* **115,** 2262–2278.